Open Research Online

Open Research Online

Looking at the bright side of the ρ Ophiuchi dark cloud[*]

Far infrared spectrophotometric observations of the ρ Oph cloud with the ISO–LWS

R. Liseau[1], **G.J. White**[2], **B. Larsson**[1], **S. Sidher**[3], **G. Olofsson**[1], **A. Kaas**[1], **L. Nordh**[1], **E. Caux**[4], **D. Lorenzetti**[5], **S. Molinari**[6], **B. Nisini**[7], and **F. Sibille**[8]

[1] Stockholm Observatory, SE-133 36, Saltsjöbaden, Sweden (rene@astro.su.se; web: www.astro.su.se/rene/)
[2] Queen Mary and Westfield College, Department of Physics, University of London, Mile End Road, London E1-4NS, UK
[3] Space Science Department, Rutherford Appleton Laboratory, Chilton Oxon OX11 OQX, UK
[4] CESR CNRS-UPS, B.P. 4346, F-31028 Toulouse Cedex 04, France
[5] Osservatorio Astronomico di Roma, Via Osservatorio 2, I-00040 Monteporzio, Italy
[6] IPAC/Caltech, MS 100-22, Pasadena, CA, USA
[7] Istituto di Fisica dello Spazio Interplanetario CNR, Tor Vergata, Via Fosso del Cavaliere, I-00133 Roma, Italy
[8] Observatoire de Lyon, F-69230 St. Genis-Laval, France

Abstract. We present far infrared (45–195 μm) spectrophotometric observations with the ISO-LWS of the active star forming ρ Oph main cloud (L 1688). The [C II] 158 μm and [O I] 63 μm lines were detected at each of the 33 positions observed, whereas the [O I] 145 μm line was clearly seen toward twelve.

The principal observational result is that the [C II] 158 μm line fluxes exhibit a clear correlation with projected distance from the dominant stellar source in the field (HD 147889). We interpret this in terms of PDR-type emission from the surface layers of the ρ Oph cloud. The observed [C II] 158 μm/[O I] 63 μm flux ratios are larger than unity everywhere. A comparison of the [C II] 158 μm line emission and the FIR dust continuum fluxes yields estimates of the efficiency at which the gas in the cloud converts stellar to [C II] 158 μm photons ($\chi_{\rm C II} \gtrsim 0.5\%$).

We first develop an empirical model, which provides us with a three dimensional view of the far and bright side of the dark ρ Oph cloud, showing that the cloud surface towards the putative energy source is concave. This model also yields quantitative estimates of the incident flux of ultraviolet radiation ($G_0 \sim 10^1 - 10^2$) and of the degree of clumpiness/texture of the cloud surface (filling of the 80$''$ beam ~ 0.2).

Subsequently, we use theoretical models of PDRs to derive the particle density, n(H), and the temperature structures, for $T_{\rm gas}$ and $T_{\rm dust}$, in the surface layers of the ρ Oph cloud. $T_{\rm gas}$ is relatively low, ~ 60 K, but higher than $T_{\rm dust}$ (~ 30 K), and densities are generally found within the interval $(1–3)\ 10^4$ cm^{-3}. These PDR models are moderately successful in explaining the LWS observations. They correctly predict the [O I] 63 μm and [C II] 158 μm line intensities and the observed absence of any molecular line emission. The models do fail, however, to reproduce the observed small [O I] 63 μm/[O I] 145 μm ratios. We examine several possible explanations, but are unable to uniquely identify (or to disentangle) the cause(s) of this discrepancy.

From pressure equilibrium arguments we infer that the total mass of the ρ Oph main cloud (2 pc^2) is $\sim 2\,500\,{\rm M}_\odot$, which implies that the star formation efficiency to date is $\lesssim 4\%$, significantly lower than previous estimates.

Key words: stars: formation – ISM: structure – ISM: general – ISM: atoms – ISM: clouds – ISM: individual objects: ρ Oph cloud

1. Introduction

The eastern, dense regions of the ρ Ophiuchi clouds (L 1688 or the ρ Oph 'main cloud') are currently in a highly active state of star formation. Observations of the young stars associated with this cloud provided the empirical basis (Wilking & Lada 1983) of what has become the standard theory of low-mass star formation (Shu et al. 1987). In this paper, we present far infrared observations of the ρ Oph cloud, which are unhindered by telluric atmospheric absorption.

The spatial resolution of the ISO-LWS (Infrared Space Observatory, see: Kessler et al. 1996; Long Wavelength Spectrometer, see: Clegg et al. 1996 and Swinyard et al. 1996) is comparable to a typical Jeans length in the ρ Oph cloud[1] and the instrument appears ideal to study the energy balance of the cloud by means of spectroscopy of the major cooling lines, viz. molecular and atomic fine structure lines in the FIR (far infrared). The wide spectral range (40–200 μm) of the LWS permits si-

[1] For fully molecular gas, $L_{\rm Jeans}(25\,{\rm K},\ 10^3\,{\rm cm}^{-3}) = 0.1$ pc, i.e. $\sim 160''$ at the distance of 150 pc; the LWS beam $\sim 80''$.

multaneously the cooling by the gas and dust components to be addressed and hence the study of the gas and dust coupling on spatial scales relevant to star formation.

The presence of early type stars which provide potential sources of external heating of the cloud can be expected to produce a PDR (Photon Dominated Region; see the review by Hollenbach & Tielens 1997). The cooling of such regions is dominated by [C II] 158 μm and/or [O I] 63 μm line emission, where the relative importance of the lines will depend on the cloud density and the flux of ultraviolet radiation. For relatively weak radiation fields, $\lesssim 10^3$ times the *Habing Field* (Habing 1968), weak-type PDRs should develop (Hollenbach et al. 1991) and, as such, the ρ Oph cloud could be expected to present a test case of models of such interface regions in the interstellar medium.

In the present contribution, we present Iso-Lws observations of the ρ Oph cloud in the far infrared (Sects. 2 and 3). The analysis of these data will naturally lead the discussion toward the topic of PDRs. However, we shall first attempt to develop an empirical model (Sects. 4.1–4.3) before comparing the results with theoretical model calculations (Sect. 4.4). In Sect. 4.5, we revisit the related issues of the mass and the star formation efficiency of the ρ Oph main cloud. Finally, in Sect. 5 we summarise our main conclusions from the present work.

2. Observations and data reductions

The observations of the ρ Oph cloud were collected with the Iso-Lws on February 12, March 16, March 22 and August 18, 1997.

We targeted 33 individual positions in the ρ Ophiuchi dark cloud, the coordinates of which are given in Table 1. Literature data for ρ Oph (e.g. maps) have traditionally been presented for the epoch 1950 and, for convenience, we provide both J 2000 and B 1950 coordinates in the table. The Lws data were obtained as spatial strip scans across the cloud as indicated in Fig. 1. The actual strip scans deviate somewhat from those originally planned: e.g., the scan designated ew is not strictly in the east-west direction but at a position angle $\sim 90^\circ.4$. Generally, offsets between consecutive positions were $180''$, except for the scan through the dense cores in ρ Oph B, where the offsets of $40''$ were intended to fully sample the nominal $80''$ beam of the Lws (Swinyard et al. 1996) in the scan direction. The pointing errors were generally less than $2''$.

A first determination of the beam size of the Lws established that it was $\sim 80''$, independent of the wavelength. However, attempts to obtain detailed maps of the beam pattern indicate that this first-cut value would need to be updated[2]. In particular, current estimates for the Lws beam (effective circular half power width) yield $83''$ at 63 μm ($1.27\,10^{-7}$ sr), $62''$ at 145 μm ($7.10\,10^{-8}$ sr), and $68''$ at 158 μm ($8.54\,10^{-8}$ sr), and which will be adopted throughout this paper.

Full Lws-spectra ($\Delta\lambda = 43$–197 μm, $R = 140$–330) were obtained at all positions, oversampling the spectral resolution by a factor of 4, and with integration times ranging from ~ 15 min

[2] See also:
http : //isowww.estec.esa.nl/instr/LWS/note/beam_mem.html

to 45 min. In particular, for the different strip scans, at each position the number of individual spectral scans of the grating and integration times on the date of observation were: **ew 1–13** (8, 1 333 s, February 12), **b 1–11** (5, 942 s, March 16), **c 1–6** (11, 1 867 s, March 22), **d 1–2** (11, 2 002 s, March 22) and **a 1** (14, 2 678 s, August 18).

The data were reduced using the Lws pipeline (OLP 7.0). Flux calibration was achieved using Uranus as primary calibrator (for details, see: Swinyard et al. 1996) and the absolute accuracy is estimated to be within 30%. This accuracy is strictly valid only for sources which are pointlike to the Lws beam (the radial distance from the optical axis $\lesssim 25''$ at the 1 dB level).

Post-pipeline processing involved reduction of the individual spectral scans ('forward' and 'backward', respectively), such as removal of spikes due to cosmic ray events ('glitches') and of fringing due to interference along the optical path within the instrument. Finally, the individual spectral scans were averaged and merged to yield a single spectrum per scan direction for each observed position.

3. Results

3.1. Far infrared fluxes observed with the Lws

#### 3.1.1. Fine structure lines

The only fine structure lines detected with confidence were [O I] 63 μm, [O I] 145 μm and [C II] 158 μm. Specifically, no lines of higher ionization states and within the Lws spectral range were present in the FIR-spectra of the ρ Oph cloud. Each of the three detected lines was registered by two individual detectors each, an advantage, which is used to confirm (or to disprove) the presence of weak spectral features. Because of the differing responsivity of the detectors, line flux measurements were made using only one detectector for each line ([O I] 63 μm: SW 3, [O I] 145 μm: LW 3 and [C II] 158 μm: LW 4; for the instrument description, see: Clegg et al. 1996). These measurements included subtraction of a low order polynomial to remove the local continuum, and integration of the flux density under the line. The line fluxes are reported in Table 2, where the associated errors refer to the rms-noise of the surrounding continuum.

3.1.2. FIR continuum emission

All of the spectra show clear evidence of FIR continuum emission across the entire spectral range of the Lws. Previous observations by IRAS were limited to the broad bands centered at 60 and 100 μm. Using three different methods of measurement the integrated FIR-flux (50–195 μm) was determined. These included (1) direct integration of the flux density for each detector and summing up the various contributions, i.e. no fitting was involved; (2) 'stitching' the individual detectors together - in order to obtain a physically more realistic description of the continuous energy distribution - by demanding the flux in each detector band be conserved; and (3) stitching of the detectors by fixing the detector LW 1 as the reference and linearly scaling (shifting)
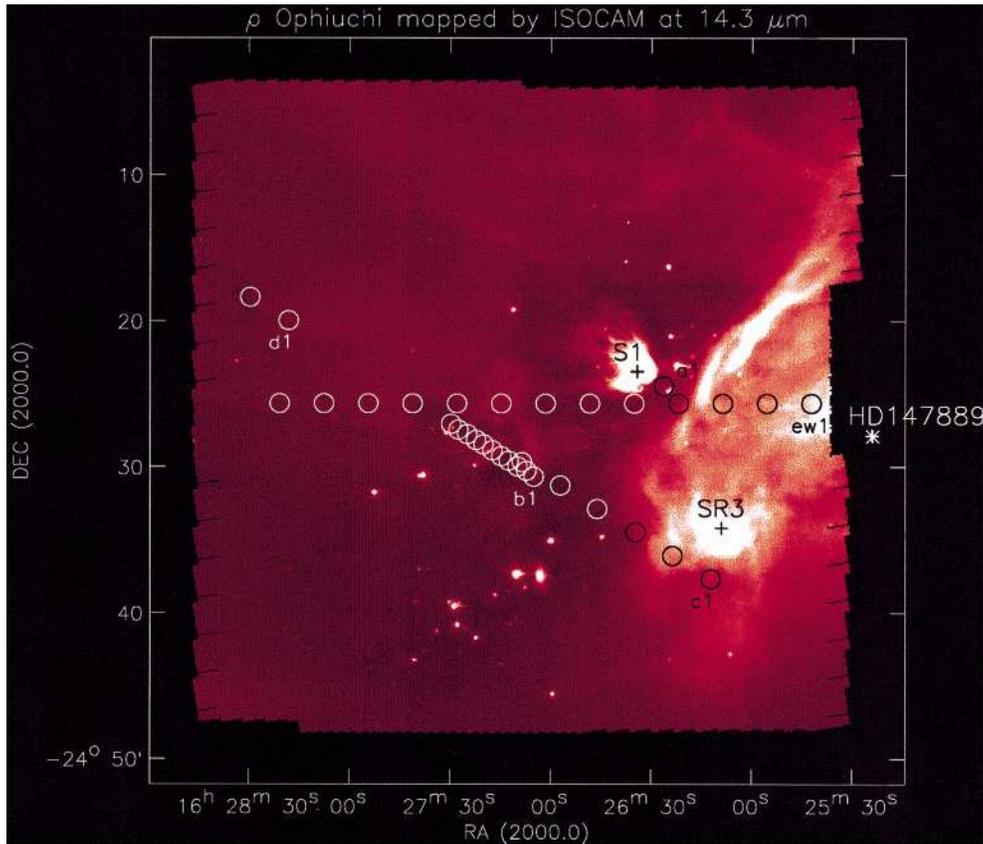
Fig. 1. Observed positions in ρ Oph superposed onto the Iso-Cam (Cesarsky et al. 1996) image by Abergel et al. 1996 (LW 3, 12–18 μm). The equatorial coordinates refer to the epoch J 2000. The size of the open symbols corresponds to the nominal beam of the Lws (80″). For each strip scan, the first pointing is indicated (see: Table 1) and the positions of the early type stars discussed in the text are shown by crosses and a star symbol

the others. Methods (2) and (3) use χ^2-minimization algorithms. All three methods gave similar results and in Table 2, the mean value, corrected for line emission (but not for missing bolometric flux), is presented. The errors quoted in the table refer to the standard deviation about this mean for each position. An average value for the far infrared intensity, $I_{\mathrm{IR}} \sim 6\,10^{-2}\,\mathrm{erg\,cm^{-2}\,s^{-1}\,sr^{-1}}$ (80″ beam), is implied by these results.

3.1.3. Molecular lines

The spectral range covered by the Lws includes a large number of (especially rotational) molecular transitions, such as those of CO ($J \geq 14$), OH (e.g. the $^2\Pi_{3/2}$ ground state transition) and H_2O (numerous lines of both ortho- and para-water). In PDRs, the presence of CO (14–13) 186 μm (and higer rotational levels) has traditionally been taken as observational evidence for the clumpiness of the media because of their high critical densities. In addition, the $(2_{12} - 1_{01})$ 179.5 μm transition to the ground state of ortho-H_2O is in principle easily excited already at low temperatures and moderate densities and could contribute significantly to the cooling of the gas. A careful search for molecular features in the ρ Oph-spectra was not successful and in no case did we detect any molecular line emission.

3.1.4. Summary of the principal results

From Table 2 it is evident that [C II] 158 μm and [O I] 63 μm emission was detected towards all 33 observed positions, whereas the [O I] 145 μm line was clearly seen towards twelve. The [C II] 158 μm flux is observed to be generally stronger than that of the [O I] 63 μm line. These lines do not exhibit any obvious correlation with the presence of dense cores in ρ Oph (Loren et al. 1990, Table 1). Also evident from Table 2 is the fact that both lines weaken moving from the western to the eastern edge of the cloud. This is also generally true for the continumm emission, if the pointings which include (or are very close to) strong FIR point sources, e.g. a 1 (VLA 1623), b 6 (IRS 37) and ew 5 (S 1), are disregarded.

3.2. Comparison with previous observations

In cases where comparisons have been possible, Lws data show generally good agreement with results obtained by, e.g., IRAS and/or the KAO (Kuiper Airborne Observatory; see also below).

[C II] 158 μm observations of ρ Oph have previously been reported by Yui et al. (1993). The general east-west gradient in intensity is clearly exhibited also by these BICE data (Balloon-borne Infrared Carbon Explorer). However, as the angular resolution of these observations was much lower (15′) than of those with the Lws, the results are as such not comparable in detail. From the large scale map presented by these authors we estimate line intensities in the range $(2\text{--}10)\,10^{-5}\,\mathrm{erg\,cm^{-2}\,s^{-1}\,sr^{-1}}$ over the region of our observations. For filled Lws beams (see: Sect. 2) our measurements imply [C II] 158 μm intensities of the order of $(8\text{--}40)\,10^{-5}\,\mathrm{erg\,cm^{-2}\,s^{-1}\,sr^{-1}}$, i.e. systematically a factor of four higher than the values determined by Yui

Table 1. Spatial scans and observed positions with the Lws of the ρ Ophiuchi main cloud

Source ID	R.A. J2000 (h)	(m)	(s)	Dec. J2000 (°)	(′)	(″)	R.A. B1950 (h)	(m)	(s)	Dec. B1950 (°)	(′)	(″)	Offset (″)	Dense Core
ew 1	16	25	42.38	–24	25	38.6	16	22	40.99	–24	18	51.8	0	
ew 2	16	25	55.56	–24	25	39.3	16	22	54.16	–24	18	53.3	180	
ew 3	16	26	8.74	–24	25	39.9	16	23	7.33	–24	18	54.8	180	
ew 4	16	26	21.92	–24	25	40.4	16	23	20.50	–24	18	56.2	180	
ew 5	16	26	35.10	–24	25	40.9	16	23	33.66	–24	18	57.5	180	
ew 6	16	26	48.28	–24	25	41.3	16	23	46.83	–24	18	58.8	180	
ew 7	16	27	1.46	–24	25	41.6	16	24	00.00	–24	19	00.0	180	
ew 8	16	27	14.64	–24	25	41.8	16	24	13.17	–24	19	1.1	180	
ew 9	16	27	27.82	–24	25	42.0	16	24	26.34	–24	19	2.2	180	
ew10	16	27	41.00	–24	25	42.1	16	24	39.50	–24	19	3.2	180	
ew11	16	27	54.18	–24	25	42.2	16	24	52.67	–24	19	4.1	180	
ew12	16	28	7.36	–24	25	42.1	16	25	5.84	–24	19	4.9	180	
ew13	16	28	20.54	–24	25	42.0	16	25	19.01	–24	19	5.7	180	
b 1	16	27	5.00	–24	30	40.2	16	24	3.43	–24	23	58.8	0	
b 2	16	27	7.49	–24	30	19.1	16	24	5.93	–24	23	37.9	40	
b 3	16	27	9.98	–24	29	57.9	16	24	8.42	–24	23	16.9	40	
b 4	16	27	12.47	–24	29	36.8	16	24	10.91	–24	22	55.9	40	ρ Oph B 1
b 5	16	27	14.95	–24	29	15.7	16	24	13.41	–24	22	35.0	40	
b 6[†]	16	27	17.44	–24	28	54.5	16	24	15.90	–24	22	14.0	40	
b 7	16	27	19.93	–24	28	33.4	16	24	18.39	–24	21	53.0	40	
b 8	16	27	22.42	–24	28	12.2	16	24	20.88	–24	21	32.0	40	
b 9	16	27	24.90	–24	27	51.1	16	24	23.38	–24	21	11.0	40	
b10	16	27	27.39	–24	27	29.9	16	24	25.87	–24	20	50.1	40	
b11	16	27	29.88	–24	27	8.8	16	24	28.36	–24	20	29.1	40	ρ Oph B 2
c 1	16	26	12.40	–24	37	41.0	16	23	10.72	–24	30	56.1	0	
c 2	16	26	23.61	–24	36	5.9	16	23	21.96	–24	29	21.8	180	
c 3	16	26	34.81	–24	34	30.8	16	23	33.19	–24	27	47.4	180	
c 4	16	26	46.01	–24	32	55.7	16	23	44.41	–24	26	13.1	180	
c 5	16	26	57.21	–24	31	20.5	16	23	55.63	–24	24	38.6	180	ρ Oph C 1
c 6	16	27	8.40	–24	29	45.2	16	24	6.84	–24	23	4.1	180	
d 1	16	28	18.00	–24	20	1.1	16	25	16.59	–24	13	24.6	0	
d 2	16	28	29.18	–24	18	25.9	16	25	27.80	–24	11	50.2	180	ρ Oph D
a 1	16	26	26.38	–24	24	30.5	16	23	24.98	–24	17	46.6	0	ρ Oph A[‡]

Notes: [†] The position is that of IRS 37 (Wilking et al. 1989).
[‡] The observations were taken towards the outflow source VLA 1623 (André et al. 1993).

et al. (1993). These authors cite the Cobe observations (COsmic Background Explorer, $7°$ beam) by Wright et al. (1991), yielding a [C II] 158 μm flux larger by more than a factor of two compared to the balloon data. Very different emission scales may be involved here and it is difficult to draw any firm conclusions (but see below).

With the Kao (beam $\sim 41''$) Ceccarelli et al. (1997) have obtained a small map in the [O I] 63 μm line around the outflow source VLA 1623 (André et al. 1993), showing that maximum flux is observed $\sim 1'$ to $2'$ northeast of the VLA position. From this map, we have tried to estimate the amount of radiation falling into the beam of the Lws, centered on the VLA source, and compared the result with our actual observation (Table 2). Although this procedure may not guarantee a conclusively reliable result, the agreement between these two values (Lws: 23 ± 2 and Kao: 18 ± 3, in units of 10^{-12} erg cm^{-2} s^{-1}) is acceptable (within $\sim 20\%$).

4. Discussion

4.1. The nature of the fine structure line emission

There are several reasons to believe that the excitation of the observed fine structure emission is caused by a source external to the ρ Oph cloud. Firstly, the emission is widespread, which makes it highly improbable that an internal source(s) in the relatively cold cloud ($T \lesssim 50$ K) could provide the necessary energy to excite the levels ($\Delta E/k = 92$ K for [C II] 158 μm and 228 K for [O I] 63 μm). Secondly, with no obvious radiative source, mechanical energy input with subsequent shock dissipation could be a viable option. However, in no case do we directly observe any of the known or suspected HH objects in the cloud (Wilking et al. 1997, Gómez et al. 1998). Furthermore, behind dense interstellar shocks the [C II] 158 μm to [O I] 63 μm intensity ratios tend to be $\ll 1$ (Hollenbach & McKee 1989), contrary to those observed in ρ Oph. Such line ratios are, how-
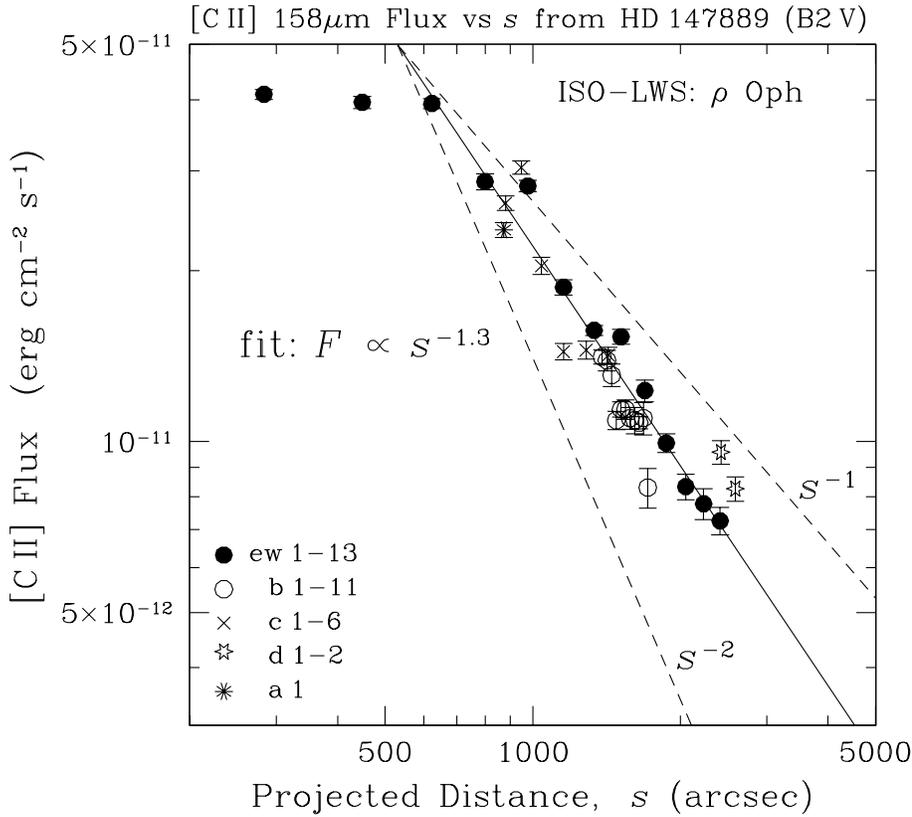
Fig. 2. The observed [C II] 158 μm flux as function of the projected distance, s, from the B2 V star HD 147889. The least squares fit to the data (with error weighting) is shown by the solid line. For comparison, the dashed lines delineate $1/s$ and $1/s^2$ dependencies, respectively. Shown error bars reflect the rms-noise of the continuum close to the line

ever, predicted by models of relatively weak PDRs (Hollenbach et al. 1991), i.e. regions of molecular clouds which are irradiated by ultraviolet (UV) radiation. Thirdly and most importantly, optically and NIR bright nebulosity near the western cloud edge hints at external illumination. Three early type stars are found in the immediate vicinity of the ρ Oph main cloud, viz. HD 147889 (B2 V), S 1 (B3 V) and SR 3 (B7 V), all of which are potential sources of UV photons capable of ionizing carbon, which is subsequently observed in the form of [C II] 158 μm line emission. Examination of the apparent distance dependence of the [C II] 158 μm line flux for each of the three B-stars results in a comprehensive pattern only for the hottest star, implying that HD 147889 completely dominates the UV-field at the ρ Oph cloud[3]. In Fig. 2, we show the [C II] 158 μm flux toward all 33 observed positions as a function of the projected angular distance, s, from the B2 V star, where

$$s = \arccos\left[\cos\delta\cos\delta_{HD} + \sin\delta\sin\delta_{HD}\cos(\alpha_{HD} - \alpha)\right]$$

with obvious notations for Right Ascension and Declination. It is evident from the figure that the majority of the data points cluster along a common locus, the equation of which has been determined from least squares fitting as

$$\log F(s) = (-1.29 \pm 0.02)\log s + (12.96 \pm 0.32)$$

when logarithms are to the base of ten and units are in erg cm^{-2} s^{-1} and cm ($D = 150$ pc), for F and s respectively.

---

[3] The [C II] 158 μm flux from the source a 1 (VLA 1623) follows this relation too (Fig. 2), in spite of the fact that it's projected location is much closer to the B3 star S 1.

The power law exponent (~ 1.3) has a value distinctly smaller than an inverse square law. A reasonable explanation is that this is an effect of viewing geometry and we argue below that this can in fact be used to (1) determine the strength of the local UV field in ρ Oph and (2) reconstruct the three dimensional distribution of the [C II] 158 μm emitting regions from the two dimensional observations. Before going ahead we have first to examine the stellar parameters of HD 147889.

4.2. The stellar model of HD 147889

As outlined in the Appendix, the basic assumption in our model is the conservation of the radiative energy from the stellar source. We used the stellar atmosphere models by Kurucz (1992) for the spectral type of HD 147889, viz. B2 V (Chini 1981), in order to determine the UV flux at the stellar surface. The atmosphere models have been computed for a variety of stellar parameters, such as pressure and chemical composition. However, the integrated UV flux between 6 eV and 13.6 eV (see below) is relatively insensitive to changes in these parameters, viz. within $\sim 2\%$, when varying the surface gravity, $\log g$, by ± 0.5 dex or when changing the metallicity, $\log(Z/Z_\odot)$, by $+0.3$ dex. Obviously, the most critical parameter is the effective temperature, T_{eff}, of the star: changing T_{eff} by $\pm 1\,000$ K about the nominal value for a B2 V star (22 000 K), results in UV flux changes of $\sim 20\%$. However, the stellar model must not produce a radiative luminosity in excess of the total observed toward the ρ Oph complex (e.g., Greene & Young 1989), an argument we used to constrain our choice of the stellar model atmosphere.
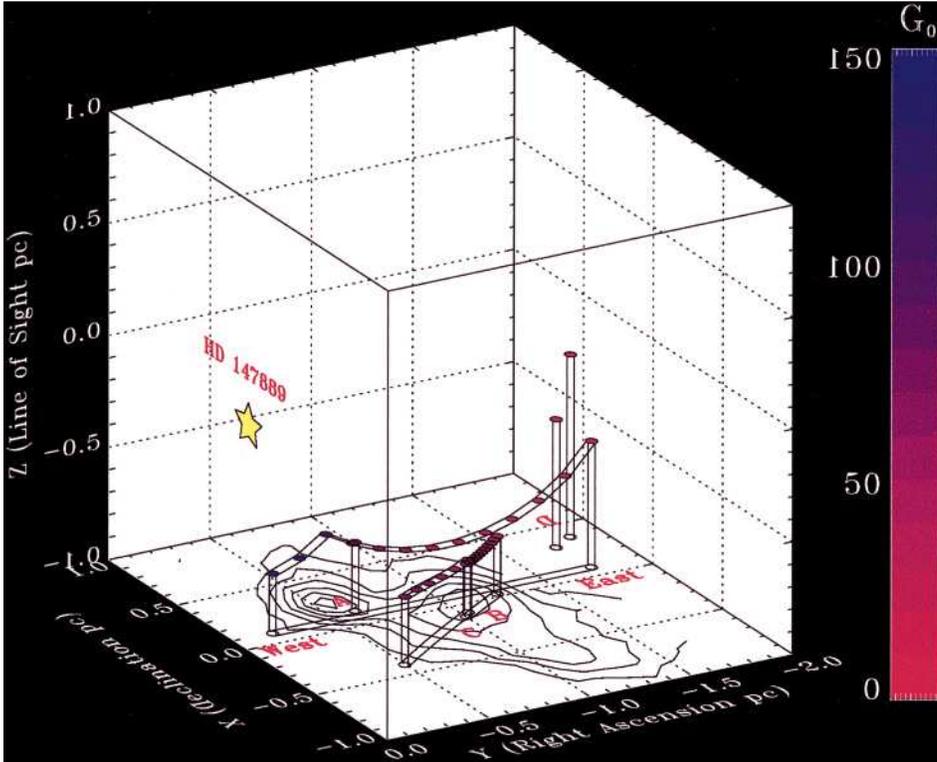
Fig. 3. Three dimensional view of the far-side environs of the ρ Oph cloud. The B2 V star HD 147889 is at the origin, the observer's line of sight along the z-axis and the plane of the sky in the xy-plane. The intensity scale of the displayed points, expressed in units of G_0 of the incident UV radiation field, is shown by the bar to the right. Connecting lines have been drawn to guide the eye. For reference, the CS (J=2–1) map from Liseau et al. (1995) is shown as contours. The actual observations have been performed from far below the bottom panel of the shown box. Notice the concave surface of the cloud, presumably caused by erosion due to the UV field and the stellar wind from the early B star

We finally adopt the Kurucz model atmosphere for $T_{\rm eff} = 22\,000$ K, $\log g = 4.0$, $\log(Z/Z_\odot) = 0.0$. The stellar radius is found as $R_\star = 5\,{\rm R}_\odot$ from matching this B2 V model to the observed fluxes at 9 μm by Hanner et al. (1995) at the adopted distance of 150 pc. This implies a bolometric luminosity $L_\star = 5\,300\,{\rm L}_\odot$ which, given the uncertainties involved, is in very good agreement with the value of $5\,500\,{\rm L}_\odot$ quoted by Wilking et al. (1989).

4.3. The UV field on the far side of the ρ Oph cloud and the texture of the medium

The deviation of the flux-distance relationship from an inverse square law (Sect. 4.1) can be naturally explained in terms of a specific geometric arrangement of the exciting stellar source, the emitting [C II] 158 μm sources and the observer, as outlined in the Appendix. There, we assume that a certain fraction, $\chi_{\rm CII}$, of the incident stellar UV luminosity is converted into [C II] 158 μm photons which are emitted isotropically. This permits us to estimate the degree of homogeneity of the emitting gas and the strength of the local UV radiation field, expressed in units of G_0, which approximately corresponds to the *Habing-Field*, integrated over $6\,{\rm eV} \leq {\rm h}\nu \leq 13.6\,{\rm eV}$ (Tielens & Hollenbach 1985a). Since the continuum is 'contaminated' by embedded stellar sources at several positions, we prefer to use for $\chi_{\rm CII}$ an average of the observed [C II] 158 μm to the Fir flux, rather than the individual ratios (Table 2). This average value, $\chi_{\rm CII} \sim 0.5\%$, is in agreement with expectation from the theory of photoelectric grain heating mechanisms in Pdrs ($\sim 10^{-3}$ to 10^{-2}, see: Hollenbach & Tielens 1997).

From the Lws observations, and for the adopted stellar model of HD 147889, this empirical model indicates that the extent of the emitting regions is typically smaller than the beam of our observation, i.e. that the beam filling factors are ~ 0.1–0.2 (average $f_{\rm beam} = 0.16$). Interpreted in terms of *single* sources, this would suggest that the diameter of a typical [C II] 158 μm source is $\gtrsim 30''$. However, we recall that the Lws data are generally quite strongly fringed, which could indicate the presence of either extended emission or an off-axis point source (or both). We are not able to distinguish between these possibilities and have to leave open, whether the [C II] 158 μm data reflect typical [C II] 158 μm scales of the order of a few tens of arcseconds, the existence of conglomerates of yet smaller clumps distributed stochastically within the Lws beam or simply small-scale texture, such as filamentary structure etc. The relative smoothness of the [C II] 158 μm distribution in ρ Oph B, which was mapped at roughly half-beam spacing, supports these latter options. In addition, the millimetre-continuum observations by Motte et al. (1998), who determined the typical scale of cold *dust* structures to be smaller than $30''$, could speak in favour of the small clump hypothesis. However, we must caution that this result is based on the assumption that the point source calibration of the Lws is applicable to the ρ Oph data presented here.

The values of G_0 derived from the model are of the order of some 10^1 to 10^2. For the seemingly saturated [C II] 158 μm sources ew 1 and ew 2 we simply assumed an average s and an r^{-2} dependence of the flux, which could of course be incorrect. Anyhow, *exact* values of G_0 are sensitive to the stellar input parameters (see: Sect. 4.2), but values as high as 10^3 can be confidently ruled out. The continuum data (Table 2) lend

Table 2. Observed FIR flux in the ρ Oph cloud

		$F_{\text{line}}^{\dagger}$		$F_{\text{cont}}^{\ddagger}$
ID	[C II] 158	[O I] 63	[O I] 145	[50, 195] μm
ew 1	40.9 ± 0.8	26.2 ± 0.7	5.4 ± 0.3	2086 ± 195
ew 2	39.6 ± 1.0	12.4 ± 0.6	4.0 ± 0.4	1411 ± 93
ew 3	39.4 ± 0.8	14.6 ± 0.5	4.9 ± 0.4	1211 ± 49
ew 4	28.7 ± 0.9	12.6 ± 0.4	3.0 ± 0.4	1126 ± 36
ew 5	28.2 ± 0.7	14.4 ± 0.5	3.8 ± 0.5	1859 ± 91
ew 6	18.7 ± 0.6	5.7 ± 0.4	< 1.7	517 ± 13
ew 7	15.7 ± 0.3	4.6 ± 0.4	< 1.3	379 ± 3
ew 8	15.3 ± 0.5	3.4 ± 0.3	0.5 ± 0.1	417 ± 3
ew 9	12.3 ± 0.5	3.2 ± 0.3	< 0.9	292 ± 2
ew10	9.9 ± 0.4	2.2 ± 0.3	< 0.7	201 ± 7
ew11	8.3 ± 0.4	1.9 ± 0.3	< 0.7	149 ± 8
ew12	7.8 ± 0.5	1.3 ± 0.2	< 0.6	110 ± 9
ew13	7.2 ± 0.4	1.2 ± 0.2	< 0.5	98 ± 6
b 1	14.1 ± 0.4	2.8 ± 0.5	< 1.4	449 ± 4
b 2	13.9 ± 0.6	2.9 ± 0.4	< 1.4	469 ± 2
b 3	13.1 ± 0.6	3.1 ± 0.6	< 1.3	492 ± 4
b 4	10.9 ± 0.4	3.8 ± 0.5	< 1.2	513 ± 5
b 5	11.4 ± 0.4	4.6 ± 0.5	< 1.5	586 ± 12
b 6	11.4 ± 0.4	4.6 ± 0.4	< 1.4	706 ± 24
b 7	11.0 ± 0.5	3.9 ± 0.6	< 1.4	651 ± 40
b 8	10.9 ± 0.6	3.3 ± 0.3	< 4.2	529 ± 23
b 9	10.8 ± 0.3	3.0 ± 0.3	< 2.1	476 ± 9
b10	11.0 ± 0.7	3.8 ± 0.4	< 3.8	656 ± 9
b11	8.3 ± 0.7	4.3 ± 0.5	< 2.4	654 ± 12
c 1	26.3 ± 0.8	6.8 ± 0.4	1.5 ± 0.1	723 ± 23
c 2	30.4 ± 0.8	6.4 ± 0.3	2.5 ± 0.2	817 ± 44
c 3	20.4 ± 0.7	3.3 ± 0.5	2.2 ± 0.4	822 ± 37
c 4	14.4 ± 0.5	1.8 ± 0.2	0.5 ± 0.1	559 ± 16
c 5	14.5 ± 0.5	2.5 ± 0.2	< 1.3	451 ± 8
c 6	14.2 ± 0.5	3.1 ± 0.3	0.3 ± 0.1	542 ± 22
d 1	9.6 ± 0.5	1.5 ± 0.2	< 0.6	136 ± 1
d 2	8.3 ± 0.4	0.7 ± 0.2	< 0.5	135 ± 2
a 1	23.6 ± 0.7	23.4 ± 1.5	1.4 ± 0.2	3519 ± 247

Notes: [†] Units are 10^{-12} erg cm^{-2} s^{-1}. Errors are statistical and upper limits $3\,\sigma$.
[‡] Continuum flux is in 10^{-11} erg cm^{-2} s^{-1} per beam and integrated between 50 and 195 μm.

Table 3. 3 D coordinates (r, θ, ϕ) and G_0 values in ρ Oph

ID	$s^{\S}$ (pc)	pa (°)	r (pc)	θ (°)	ϕ (°)	$F_{\text{UV}}^{\dagger}$ (G_0)	Dense Core
ew 1	0.21	63	0.76	164	296	129	
ew 2	0.33	74	0.76	154	285	129	
ew 3	0.45	78	0.76	143	281	131	
ew 4	0.58	81	0.89	139	278	95	
ew 5	0.71	83	1.01	135	276	73	
ew 6	0.84	84	1.13	131	275	59	
ew 7	0.97	85	1.24	128	274	49	
ew 8	1.10	85	1.34	124	274	41	
ew 9	1.23	86	1.44	121	273	36	
ew10	1.36	86	1.54	117	273	31	
ew11	1.49	86	1.63	113	273	28	
ew12	1.62	87	1.72	109	272	25	
ew13	1.75	87	1.81	104	272	23	
b 1	1.01	96	1.27	127	263	46	
b 2	1.03	95	1.28	126	264	45	
b 3	1.05	94	1.30	126	265	44	
b 4	1.08	93	1.32	125	266	43	ρ Oph B 1
b 5	1.10	93	1.34	124	266	41	
b 6	1.12	92	1.36	124	267	40	
b 7	1.15	91	1.38	123	268	39	
b 8	1.17	90	1.40	122	269	38	
b 9	1.20	90	1.41	122	269	37	
b10	1.22	89	1.43	121	270	36	
b11	1.25	88	1.45	120	271	35	ρ Oph B 2
c 1	0.64	129	0.95	137	230	84	
c 2	0.69	119	0.99	135	240	76	
c 3	0.76	110	1.05	134	249	67	
c 4	0.84	104	1.13	131	255	59	
c 5	0.93	98	1.21	129	261	51	ρ Oph C 1
c 6	1.04	94	1.29	126	265	45	
d 1	1.76	79	1.81	103	280	22	
d 2	1.88	78	1.89	95	281	20	ρ Oph D
a 1	0.64	77	0.94	137	282	85	ρ Oph A

Notes: [§] All length scales refer to the distance $D = 150$ pc.
[†] For average beam filling $f_{\text{beam}} = 0.16$ and the adopted stellar parameters for HD 147889 (see: Sect. 4.2).

support to this conclusion, since values of that order can be directly inferred from the observations, viz. G_0 about 45 to 250 ($I_{\text{IR}}/2.6\,10^{-4}$ erg cm^{-2} s^{-1} sr^{-1}), which includes contributions from other sources.

The results of our empirical model are summarised in Table 3. This table contains also the coordinates of the observed [C II] 158 μm sources in three dimensional space. There, the exciting star is at the origin of the coordinate system. Since, when observed from the Earth, many regions in the ρ Oph cloud appear dark (Abergel at al. 1996), we place the star behind the cloud, so that all z-coordinates become negative and all polar angles, θ, larger than 90°. The [C II] 158 μm emission permits us, therefore, to view the far side of the cloud. This is visualised in Fig. 3, where one can see that the overall shape of the ρ Oph cloud facing towards HD 147889 has a concave curva-

ture. This is qualitatively in agreement with expectation, if the cloud is eroded or ablated by the stellar radiation field and/or a stellar wind.

Abergel et al. (1998) provide CAM-isophotes of the dense core ρ Oph D, which suggest the illuminating source is situated toward the west, in agreement with what can be discerned from Fig. 3. In addition, the outer density of the core determined by these authors is in quantitative agreement with the results of model calculations described in the next section (see also: Fig. 4).

4.4. Theoretical PDR model calculations

#### 4.4.1. The code: CLOUDY 90 with updates

For the ρ Oph cloud PDR, we computed grids of stationary, steady state models using the publicly available photoionisa-

Table 4. Analytical fits to collisional de-excitation rate constants for $O^0\ ^3P_{j'} \rightarrow\ ^3P_j$

Transition	Radiation Wavelength (μm)	e^- $a^\dagger$	$b^\dagger$	He^0 (^1S) a	b	H_2 (J=1,0) $a^\ddagger$	$b^\ddagger$	H^0 ($^2S_{1/2}$) a	b	References
$^3P_0 \rightarrow\ ^3P_1$	145.52548	1.35	–8.74	1.41	–14.60	1.19	–13.98	0.43	–10.84	(1), (2), (3), (4), (5)
$^3P_0 \rightarrow\ ^3P_2$	44.06	0.50	–4.30	0.67	–11.56	0.33	–10.30	0.80	–11.96	(2), (3), (4), (5)
$^3P_1 \rightarrow\ ^3P_2$	63.18371	0.46	–3.83	0.69	–11.80	0.34	–10.52	0.65	–11.30	(1), (2), (3), (4), (5)

Notes: † These values refer to the collision strength $\Omega_{j,j'}$, such that $\gamma_{j',j} = 8.629\,10^{-6}\,\Omega_{j,j'}/(g_{j'}\,T^{0.5})$ and $E_{j'} > E_j$.
‡ Rates have been weighted by thermal populations of the ortho (J = 1) and para (J = 0) ground states of H$_2$ at the corresponding temperatures.
References: (1) Kaufman & Sugar (1986), (2) Bell et al. (1998), (3) Monteiro & Flower (1987), (4) Jaquet et al. (1992), (5) Launay & Roueff (1977).
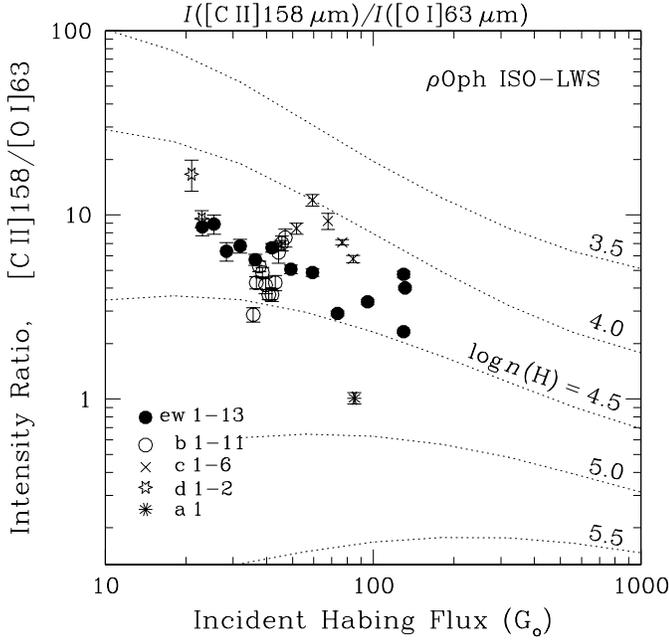
Fig. 4. The observed intensity ratios of [C II] 158 μm to [O I] 63 μm are shown vs the UV flux in G_0 from Table 3. Also displayed are the results from theoretical PDR model calculations for various values of the particle density, n(H), in cm^{-3} (see: the text)

Table 5. Parameters of the ρ Oph PDR

Parameter	Value
n(H) (cm^{-3})	$3\,10^4 – 10^5$
$G_0^\dagger$	20–140
$\zeta_{X,CR}$ (s^{-1})	$4\,10^{-17}$
F_{IR} (erg cm^{-2} s^{-1})	0.5
T_{dust} (K)	25
ξ_{turb} (km s^{-1})	1.5
a(C)‡	$1.4\,10^{-4}$
a(N)	$7.9\,10^{-5}$
a(O)	$3.0\,10^{-4}$
a(Na)	$2.3\,10^{-7}$
a(Mg)	$1.1\,10^{-6}$
a(Si)	$1.7\,10^{-6}$
a(P)	$1.2\,10^{-7}$
a(S)	$2.8\,10^{-5}$
a(Cl)	$1.9\,10^{-7}$
a(Ar)	$1.2\,10^{-6}$
a(Fe)	$1.7\,10^{-7}$

Notes: † Equivalent *Habing-Fields* in units of $1.6\,10^{-3}$ erg cm^{-2} s^{-1}.
‡ Abundances a are relative to hydrogen nuclei and only species with $a > 10^{-7}$ are listed (from: Savage & Sembach 1996).

tion code CLOUDY, version 90.04 (Ferland 1996, Ferland et al. 1998), with some appropriate changes and updates. The standard model of the Orion PDR by Tielens & Hollenbach (1985b) served as a reference when running tests of the code.

Some of the chemical reaction rates for CH$^+$ have been updated in accordance with Table 1 of Bertoldi (1998)[4]. For atomic carbon and oxygen, the more recent Einstein A values of Galavís et al. (1997) were adopted. More important though seemed the incorporation of the relevant collision processes for the excitation of the fine structure levels at relatively low temperatures in largely molecular gas. This is particularly important for O I, the ground state levels of which are inverted. The $^3P_2$ level is at zero energy, whereas the $^3P_1$ level is at $E/k = 228$ K and $^3P_0$ at

---

[4] For the relatively low temperatures of the ρ Oph PDR this is of little importance.

326 K above ground, respectively. Low-temperature collision rates with electrons (below 3 000 K) were obtained from the new results by Bell et al. (1998) and for collisions with atomic hydrogen the rates provided by Launay & Roueff (1977) were used. Monteiro & Flower (1987) computed the rate constants for helium and found that the collisional transition $^3P_0$–$^3P_1$ is considerably less probable (by up to two orders of magnitude) than the $^3P_0$–$^3P_2$ and $^3P_1$–$^3P_2$ transitions. These authors noted that $^3P_0$–$^3P_1$ transitions are collisionally forbidden to first order and pointed out that this should also be true for collisions with molecular hydrogen in an anologous way (see also the collision strengths for electrons, Bell et al. and Table 4). This was confirmed by the calculations by Jaquet et al. (1992) for the interactions of O^0 with ground state para- and ortho-H$_2$. As CLOUDY does not distinguish between different nuclear spin states in molecules, we used the rate constants of Jaquet et al. for 'hybrid H$_2$', where the weighting was done by considering
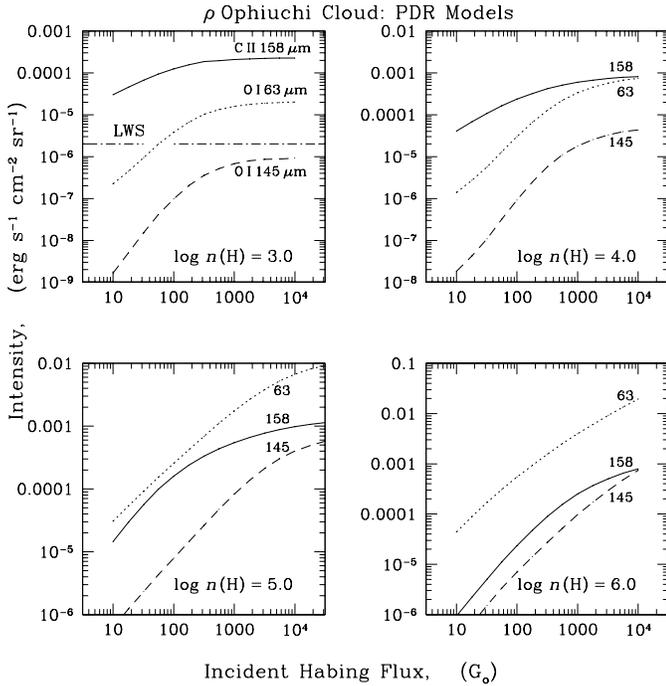
Fig. 5. Emission line intensities for [C II] 158 μm, [O I] 63 μm and [O I] 145 μm from Pdr models described in the text. The line intensities, obtained from the Cloudy flux as $F_{\mathrm{line}}/2\pi$ (see: Sect. 4.4.4), are shown as a function of G_0 for four values of the density. In the first panel (*upper left*) the sensitivity of our Lws observations is indicated by the dash-dotted line
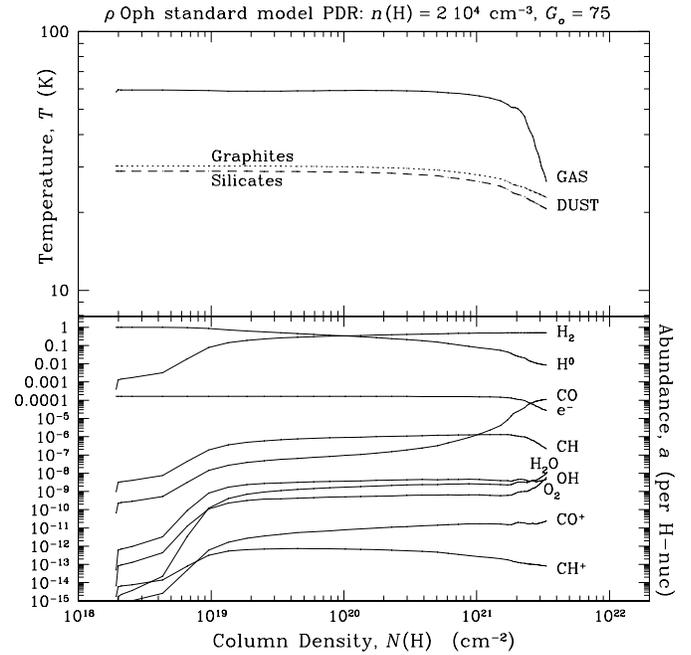

Fig. 6. Pdr model of the ρ Oph cloud for $n(\mathrm{H}) = 2\,10^4\,\mathrm{cm}^{-3}$ and $G_0 = 75$. In both graphs, the abscissa represents the column density of hydrogen nuclei, $N(\mathrm{H})$, in cm^{-2}. The *upper* panel shows the run of gas and dust temperatures into the Pdr, where the dust is considered a mixture of graphite and silicate particles. The *lower* panel displays the abundance distribution of hydrogen, electrons and molecules into the Pdr. The shown abundances are relative to the number of H-nuclei

the thermal distributions of the two forms at the corresponding temperatures. Using the rotational constants of Bragg et al. (1982), the energy difference between the $J = 0$ and $J = 1$ states is $E/k = 170.4\,\mathrm{K}$.

Analytical fits to the de-excitation rate coefficients are given in Table 4. The corresponding excitation rate constants follow from detailed balance arguments.

Self-shielding of H_2 and CO against photodissociation was accounted for with the formalism of Draine & Bertoldi (1996, Eq. 37) and of Bertoldi (1998, Eq. 7; see also Rentzsch-Holm et al. 1998). For dust shielding, the values given by Tielens & Hollenbach (1985a, their Table 5) were adopted.

4.4.2. Parameters of the Pdr models

Some of the parameters were held fixed for all of the model runs (cf. Tielens & Hollenbach 1985a, b). These included the hydrogen ionization rate due to diffuse X-rays (and cosmic rays), $\zeta_{\mathrm{X,CR}} = 4\,10^{-17}\,\mathrm{s}^{-1}$ (Casanova et al. 1995), which is double the rate adopted by Cloudy from Tielens & Hollenbach (1985a), see: *Hazy*, Ferland (1996); the relative chemical abundances, adopted from Savage & Sembach (1996) and referring to the ζ Oph line of sight (cool phase, their Table 5); the composition and size distribution of the dust grain mixture, giving rise to large values of the total-to-selective extinction, i.e. in ρ Oph, $A_{\mathrm{V}}/E_{\mathrm{B-V}} \sim 4$ when $N(\mathrm{H\,I} + 2\,H_2)/A_{\mathrm{V}} = 1.9\,10^{21}\,\mathrm{cm}^{-2}\,\mathrm{mag}^{-1}$ (Whittet et al. 1976, Bohlin et al. 1978, Savage & Mathis 1979,

Frerking et al. 1982, Wilking & Lada 1983, Vrba et al. 1993); the colour temperature of the dust, $T_{\mathrm{dust}} = 25\,\mathrm{K}$ (Greene & Young 1989, Liseau et al. 1995); the total far infrared flux, $F_{\mathrm{IR}} = 0.5\,\mathrm{erg\,cm}^{-2}\,\mathrm{s}^{-1}$ (our present Lws data; see also: Greene & Young 1989); and the turbulent velocity parameter, $\xi_{\mathrm{turb}} = 1.5\,\mathrm{km\,s}^{-1}$, estimated from observed line widths (Wilking & Lada 1983, Frerking et al. 1989, Loren et al. 1990, Liseau et al. 1995, unpublished data of R. Liseau). These Pdr model parameters of the ρ Oph cloud are summarised in Table 5.

The quantities which were varied are the incident UV-field, expressed in the G_0 scale ($1.6\,10^{-3}\,\mathrm{erg\,cm}^{-2}\,\mathrm{s}^{-1}$: Tielens & Hollenbach 1985a), and the hydrogen nucleus density $n(\mathrm{H})$. The basic Pdr-parameter, $G_0/n(\mathrm{H})$, was explored in the range $10^{-6} \leq G_0/n(\mathrm{H}) \leq 10^2\,\mathrm{cm}^3$ (for the various forms of the *Habing-Field* occurring in the literature, see: Draine & Bertoldi 1996, their Table 1). The model solves for the temperature and chemical structure of the Pdr and computes, using the escape probability formalism, the emergent line flux from the Pdr-surface (in $\mathrm{erg\,cm}^{-2}\,\mathrm{s}^{-1}$) for a large number of species (atoms, ions and molecules). The inward calculations of the cloud structure were artificially stopped at the lowest gas temperature of 10 K, beyond which Cloudy cannot reliably calculate the CO transfer. Alternatively, Cloudy stops, once the fraction of carbon tied up in molecules exceeds the 80% level.

In the ρ Oph cloud, the emission spectrum of Pahs (Polycyclic Aromatic Hydrocarbons) has been obtained by Boulanger et al. (1996), using Iso-Cam and toward a position north of the
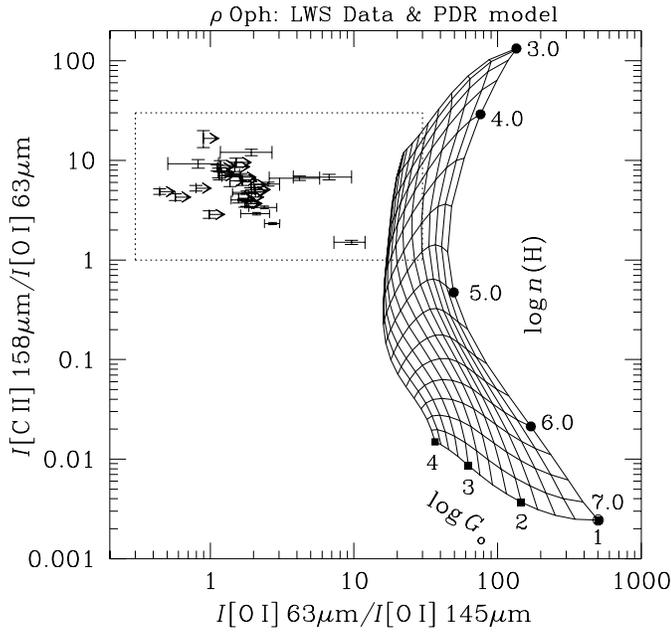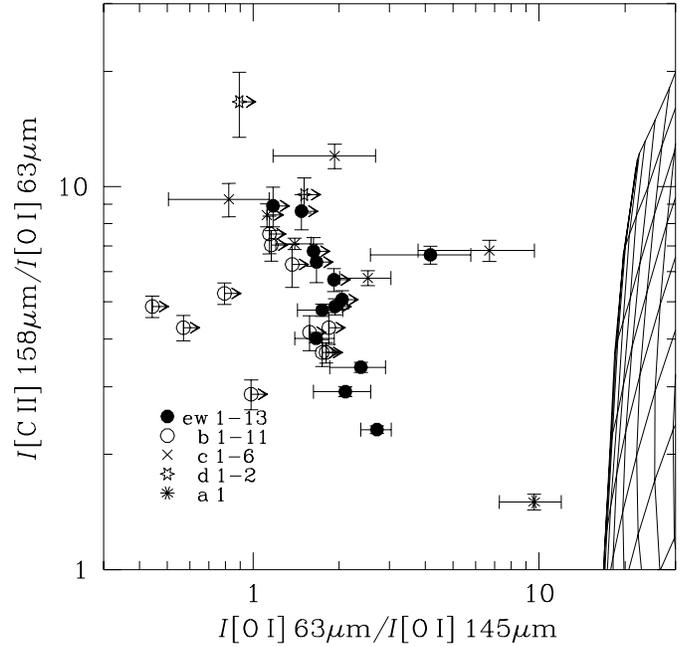
Fig. 7. Diagnostic line ratio diagram for [C II] 158 μm, [O I] 63 μm and [O I] 145 μm for the ρ Oph-PDR models described in the text. n(H) increases top-down and G_0 right-left. The logarithmic mesh of the web is 0.25 dex and parameter values are indicated at full decades. Whereas plausible models predict [O I] 63 μm/[O I] 145 μm ratios much larger than ten, the Lws observations, enclosed by the dotted box, fall generally short of that theoretical value. The box is shown enlarged in Fig. 8

Fig. 8. A blow-up of Fig. 7 (the dotted box). Non-detections of [O I] 145 μm are shown for 1 σ and result in lower limits on the oxygen line ratio. The observed strip scans are collectively identified by the symbols shown in the lower left corner. Models of the ρ Oph PDR are off scale to the right of the figure

large mosaic displayed in Fig. 1. The Pahs could affect the photoelectric heating rate (Hollenbach & Tielens 1997 and references therein) and the chemistry of the Pdr (Bakes & Tielens 1998). However, for the ρ Oph model runs, inclusion of Pahs had only marginal effects on the heating rate (see also Hollenbach et al. 1991). In Cloudy, non-homogeneous density distributions can, in principle, be opted for. For the ρ Oph cloud, such versatility would be of particular interest as the existence of inhomogeneities (clumps) is observationally well documented (e.g., Loren et al. 1990, Motte et al. 1998), and was also indirectly inferred from our Lws observations (Sect. 4.3). However, the 1D code Cloudy does, in the 'clumpy case', not treat the radiative transfer adequately. In what follows we concentrate, therefore, on homogeneous models, bearing in mind that these are at best only able to represent average cloud conditions. The modeling of clumpy Pdrs is discussed in greater detail by, e.g., Spaans (1996) and by Störzer et al. (1996).

4.4.3. Pdr modeling results for the ρ Oph cloud

Comparing the results of the Pdr models with the observed line intensities and [C II] 158 μm/[O I] 63 μm ratios, volume densities $10^4 \lesssim n(\text{H}) \lesssim 10^5$ cm^{-3} and G_0 values ~ 10 to 10^2 are indicated (Figs. 4 and 5). These results are basically in agreement with those obtained by Hollenbach et al. (1991), who had previously modeled low density, low G_0 Pdrs. From Fig. 5 it is evident that, for *any* value of G_0, a) particle densities

higher than 10^4 cm^{-3} are needed to render the [O I] 145 μm line detectable with the Lws and, b) the observed line ratios [C II] 158 μm/[O I] 63 μm are all larger than unity, implying (beam averaged) densities lower than 10^5 cm^{-3}. An example for $n(\text{H}) = 2\,10^4$ cm^{-3} and $G_0 = 75$ is shown in Fig. 6, and with all other parameters as in Table 5. In the figure, graphs of the gas and dust temperature structure and of the relative chemical abundance distribution are shown. Both the gas and the dust temperature display rather flat distributions, with $T_{\text{gas}} > T_{\text{dust}}$ throughout the Pdr. Very similar temperatures have previously been inferred from CO and Iras observations (Loren et al. 1980, Greene & Young 1989, Liseau et al. 1995). Also apparent from Fig. 6 is the rapid conversion of atomic hydrogen into molecules; half of the hydrogen is molecular for a column density $N(\text{H}) \sim 3\,10^{19}$ cm^{-2} into the Pdr. Whereas virtually all carbon has been locked up in CO at $N(\text{H}) \sim 2.5\,10^{21}$ cm^{-2}, oxygen remains almost entirely atomic throughout the Pdr. The Pdr model is consistent with our Lws spectra, in that it correctly predicts that no molecular lines should be seen. The gas becomes insufficiently warm (or dense) to appreciably excite high-J CO lines and the predicted OH and H$_2$O abundances are too low to allow these species to be detected with the Lws.

Frerking et al. (1989) have reported observations of the ρ Oph cloud in the [C I] 609 μm line. Four positions observed by these authors are within about 2′ of those observed with the Lws, viz. their sources ρ Oph A, ρ Oph B, R 35 and R 38. Assuming unit filling of their 2″7 beam, we estimate from these data, line intensities $I(609) \sim (1–3)\,10^{-6}$ erg cm^{-2} s^{-1} sr^{-1}. This is in excellent agreement with the predictions of our ρ Oph models.

These yield essentially the same values, a result which should however be viewed with some caution, since the fine structure lines of atomic carbon seem to have a low PDR-diagnostic value. In addition, the assumption of unit beam filling is speculative.

4.4.4. Observed and calculated [O I] 63, 145 μm intensities

The model is unable to reproduce the observed oxygen line ratios, i.e. model predictions are generally [O I] 63 μm/[O I] 145 μm $\gg$ 10, whereas the observed ratios are significantly smaller than this value (Figs. 7 and 8). This line ratio has been known for some time to be 'troublesome' (see, e.g., the discussion by Tielens & Hollenbach 1985b). Specifically for the ρ Oph model, it is necessary to account for the apparently 'well-behaved' [C II] 158 μm and [O I] 63 μm intensities, originating from two different chemical species, at the same time as explaining why the observed fluxes from the same atom ([O I] 63 μm and [O I] 145 μm) are not satisfactorily reproduced. Below, we consider a number of possibilities which could be the cause of this line ratio anomaly.

It could be argued that the fact that the oxygen lines were observed with different detectors could account for much of the (apparent) [O I] 145 μm excess, i.e. that the calibrations were far outside the claimed accuracy (Sect. 2). Furthermore, the presence of fringes in the spectra could add considerably to the flux uncertainty. We have carefully checked the data and concluded that the observed anomaly cannot be explained by these reasons alone.

On the basis of observations of a variety of astronomical objects, Saraceno et al. (1998) concluded that a considerable range of observed [O I] 63 μm/[O I] 145 μm line ratios exists, ranging from about 1 to $\gg$ 10. Small values are not uncommon, particularly in molecular cloud environments. This is also inferred from Table 1 of Keenan et al. (1994) who compiled line ratio data obtained with the KAO (Kuiper Airborne Observatory).

One of the classical errors when calculating line strengths is the use of inaccurate atomic data and/or inadequately accounting for atomic processes. As outlined in Sect. 4.4.1 we have taken great care to improve on these aspects of CLOUDY, and particularly of the collision processes at the low temperatures encountered in the ρ Oph PDR. However, comparing our models with those of Tielens & Hollenbach (1985b: high density, high G_0) or of Hollenbach et al. (1991: low density, low G_0), the situation has actually become worse; our models predicting even larger line ratios than given using the older rates. This is due to the much higher critical density (by up to two orders of magnitude) of the 145 μm transition compared to that of 63 μm.

Another reason of failure could be radiative transfer effects in the oxygen lines (see, e.g., also Tielens & Hollenbach 1985b). These should however have been properly taken into account by the models, since for cases of interest [O I] 63 μm is generally optically thick, whereas the optical depth in the [O I] 145 μm line is typically much less than unity. The viewing geometry could come into play here, when converting flux at the plane parallel model surface to an observed specific intensity, but would make matters even worse, since the cosine of the viewing angle is generally greater than 0.5 (See: Tables 2 and 3)[5]. Further, the [O I] 63 μm line is not very optically thick (for instance, in the ρ Oph 'standard model' of Fig. 6, τ_{63} = 1.8), reducing any geometric effects on the line ratio. Even in the extreme (and unrealistic) case of purely thermal line broadening (line widths of about 0.2 km s^{-1}), resulting in maximum opacity in the lines (τ_{63} = 11 and τ_{145} = 0.04), the theoretical oxygen line ratio would still be as large as 20. Observations of velocity resolved line profiles would be useful in this context.

It is conceivable that the assumption of homogeneity could be of critical consequence for the line ratios. However, as pointed out before, the LWS data do not show any obvious correlation with the presence of known dense clumps. This is true for both [C II] 158 μm/[O I] 63 μm and [O I] 63 μm/[O I] 145 μm, indicating that these ratios are not particularly sensitive to enhanced column densities of cold neutral material. We are aware of only a few published PDR models for which the intensities of the oxygen lines are explicitly reported. For instance, Burton et al. (1990) considered the effects of clumps in PDRs and their models could, as such, provide a good test case. These clumpy PDR models have been calculated under the assumption that the results from 1-dimensional homogeneous models can be scaled and mixed in proportions appropriate to fit observed line strengths. However, none of these models predict line ratios smaller than ten (see also Figs. 7, 8) and it seems thus unlikely that the presence of clumps is a general solution to the oxygen line problem.

The ρ Oph cloud is known to harbour an appreciable population of X-ray sources (Casanova et al. 1995 and references therein) giving rise to an extra component of diffuse radiation which has not directly been considered by our models. It seems not unreasonable to suspect that this extra field could affect the excitation of the O^0 levels. The effects of X-rays on PDRs have been theoretically investigated by Maloney et al. (1996). However, none of their models produces any remarkably small [O I] 63 μm/[O I] 145 μm ratios.

Time dependent effects in PDRs have been studied by, e.g., Hollenbach & Natta (1995) and Störzer & Hollenbach (1998). However, none of these models is directly applicable to the physical conditions prevailing in the ρ Oph cloud. In addition, no [O I] 145 μm intensities were reported.

To conclude, we are not able to identify any convincing explanation for the mismatch between theoretical and observed [O I] 63 μm/[O I] 145 μm line ratios. (Much) too low model temperatures and/or inadequate treatment of the radiative transfer in the lines might come closest (larger τ_{63} and τ_{145}, in particular), but needs still to be demonstrated. In addition, the predictable behaviour of [C II] 158 μm/[O I] 63 μm would then be difficult to understand. Slight masing in the $^3P_0$–$^3P_1$ transition could be a possible explanation, however. This would require suprathermal excitation of the $^3P_0$ level by some, yet to be identified,

---

[5] $(I_{63}/I_{145})_{obs} \sim (I_{63}/I_{145}) \times 2 \cos\theta$, where θ is the angle between the normal to the surface and the line of sight (see, e.g., Hollenbach et al. 1991).

pumping mechanism and must, therefore, at this moment be considered speculative.

4.5. Star formation in the ρ Oph cloud

At the surface of the cloud, the 'standard' PDR model yields particle densities and temperatures of the order of $2\,10^4\,\mathrm{cm}^{-3}$ and $\gtrsim 50\,\mathrm{K}$, respectively, so that the thermal gas pressure $\sim 1\,10^6\,\mathrm{cm}^{-3}\,\mathrm{K}$. As temperatures deeper into the cloud are generally lower ($\lesssim 25\,\mathrm{K}$), thermal pressure equilibrium would require average particle densities $n(\mathrm{H}) \gtrsim 4\,10^4\,\mathrm{cm}^{-3}$ for the bulk of the cloud. This result is identical to that found by Liseau et al. (1995: $n(\mathrm{H}_2) \sim 2\,10^4\,\mathrm{cm}^{-3}$) from molecular line observations (for the assumed CS abundance $X(\mathrm{CS}) = 1.0\,10^{-9}$) and implies a mass of the ρ Oph main cloud of about $2\,500\,\mathrm{M}_\odot$, with the DCO$^+$ clumps (Loren et al. 1990) contributing $\sim 10\%$. For the total mass of the young stars associated with the $2\,\mathrm{pc}^2$ core of the ρ Oph cloud ($\lesssim 10^2\,\mathrm{M}_\odot$), the star formation efficiency in the ρ Oph cloud is then slightly below the 4% level. This is significantly less than has previously been claimed in the literature. On the contrary, this efficiency compares well to that generally observed for galactic clouds and casts doubt on the relevance of the opposing concepts of 'cluster mode' and 'isolated' star formation (Lada et al. 1993 and references therein).

5. Conclusions

The main conclusions from this work can be summarised as follows:

- Iso-Lws observations of the ρ Oph cloud have revealed the presence of widespread [C II] 158 μm, [O I] 63 μm and FIR continuum emission.
- Our principal observational result is the correlation between the observed [C II] 158 μm flux and the projected distance to the B 2 star HD 147889. The flux dependence on the projected distance is shallower than an inverse square law.
- The observed angular distribution of the [C II] 158 μm line flux has enabled us to reconstruct the 3 D distribution of the line emitting regions in ρ Oph, showing that the cloud surface towards the putative energy source is concave.
- This model also provides an estimate of the local UV flux at the cloud ($G_0 \sim 20$–140) and of the degree of inhomogeneity of the cloud (0.2 filling of the 80″ beam).
- From the comparison of the Lws data with detailed models of PDRs we infer that beam averaged particle densities in the thin surface layers (A_V a few magnitudes) of the ρ Oph cloud are typically above $10^4\,\mathrm{cm}^{-3}$ but rarely as high as $10^5\,\mathrm{cm}^{-3}$.
- These models lend support to the the mass estimate of the core of the ρ Oph cloud of Liseau et al. (1995), viz. $\sim 2\,500\,\mathrm{M}_\odot$. For the known associated stellar mass content, the star formation efficiency is therefore $\lesssim 4\%$, i.e. significantly less than that commonly quoted in the literature.

Appendix A: the [C II] 158 μm PDR emission in three dimensions

In spherical polar coordinates (r, θ, ϕ), with the stellar source of ultraviolet radiation at the origin, the regions of [C II] 158 μm emission are situated at (x, y, z), viz.

$$
\begin{aligned}
x &= r \cos\phi \sin\theta = s \cos\phi \\
y &= r \sin\phi \sin\theta = s \sin\phi \\
z &= r \cos\theta
\end{aligned}
\tag{A1}
$$

where $r = \sqrt{x^2 + y^2 + z^2}$ is the true radial distance and $s = r\sin\theta$ the observed projection onto the plane of the sky (xy-plane). The z-axis is along the line of sight and the azimuthal angle ϕ is given by the observed position angle, p. The observable s is also given by (see: Sect. 4.1)

$$
s = r\sin\theta = \left[\frac{F(s)}{F(s=1)} \right]^{-\frac{1}{\alpha}}
\tag{A2}
$$

so that

$$
\begin{aligned}
x &= \left[\frac{F(s)}{F(s=1)} \right]^{-\frac{1}{\alpha}} \cos(-p) \\
y &= \left[\frac{F(s)}{F(s=1)} \right]^{-\frac{1}{\alpha}} \sin(-p)
\end{aligned}
\tag{A3}
$$

The local line flux, $F(s)$, is related to the stellar source through a luminosity ℓ, viz.

$$
\ell = F(s)\, r^2
\tag{A4}
$$

Combining $r^2 = x^2 + y^2 + z^2$ with $r^2 = F(s)/\ell$ and inserting Eqs. (A3) we find for the z-coordinate

$$
z = \left\{ \frac{\ell}{F(s)} \left[1 - \frac{[F(s)]^{1-\frac{2}{\alpha}}}{[F(s=1)]^{-\frac{2}{\alpha}} \ell} \right] \right\}^{1/2}
\tag{A5}
$$

and for the polar angle θ

$$
\cos\theta = \left\{ 1 - \frac{[F(s)]^{1-\frac{2}{\alpha}}}{[F(s=1)]^{-\frac{2}{\alpha}} \ell} \right\}^{1/2}
\tag{A6}
$$

The local values of the luminosity ℓ are determined from energy conservation considerations. The fraction of the stellar UV luminosity intercepted by the [C II] 158 μm-source at r is given by

$$
\epsilon_{\mathrm{C\,II}} = \frac{\omega_{\mathrm{C\,II}}}{4\pi} L_{\mathrm{UV}}(T_{\mathrm{eff}}, R_\star)
\tag{A7}
$$

where

$$
L_{\mathrm{UV}}(T_{\mathrm{eff}}, R_\star) = 4\pi R_\star^2\, F_{\mathrm{UV}}(T_{\mathrm{eff}}) \quad \text{and} \quad \omega_{\mathrm{C\,II}} = \frac{area}{r^2}
\tag{A8}
$$

The size of the [C II] 158 μm source is approximated by $area \sim \pi R_{\mathrm{C\,II}}^2$. A fraction $\chi_{\mathrm{C\,II}}$ of this intercepted stellar UV-luminosity is radiated isotropically in the [C II] 158 μm line, so that

$$\chi_{\mathrm{C\,II}}\,\epsilon_{\mathrm{C\,II}} = \chi_{\mathrm{C\,II}}\,\pi \left(\frac{R_{\mathrm{C\,II}}}{r}\right)^2 R_\star^2\,F_{\mathrm{UV}}(T_{\mathrm{eff}}) \qquad (A9)$$

Hence, at distance D, the observed line flux is

$$f_{\mathrm{C\,II}} = \frac{\chi_{\mathrm{C\,II}}}{4} \left(\frac{R_{\mathrm{C\,II}}}{D}\right)^2 \left(\frac{R_\star}{r}\right)^2 F(G_0) \qquad (A10)$$

where the stellar UV-flux, $F_{\mathrm{UV}}(T_{\mathrm{eff}})$, has been expressed in units of G_0 ($1.6\,10^{-3}$ erg cm^{-2} s^{-1}). The source fills a fraction f_{beam} of the Lws beam, i.e. $\pi R_{\mathrm{C\,II}}^2/D^2 = f_{\mathrm{beam}}\,\Omega_{\mathrm{beam}}$, so that Eq. (A10) reduces to

$$f_{\mathrm{C\,II}} = \chi_{\mathrm{C\,II}}\,f_{\mathrm{beam}}\,\frac{\Omega_{\mathrm{beam}}}{4\pi}\,F(G_0) \qquad (A11)$$

With the definition of ℓ in Eq. (A4) one finds that

$$\ell = \chi_{\mathrm{C\,II}}\,f_{\mathrm{beam}}\,\frac{\Omega_{\mathrm{beam}}}{4\pi}\,R_\star^2\,F_{\mathrm{UV}}(T_{\mathrm{eff}}) \qquad (A12)$$

and

$$\ell = \chi_{\mathrm{C\,II}}\,f_{\mathrm{beam}}\,\frac{\Omega_{\mathrm{beam}}}{4\pi}\,r^2\,F(G_0) \qquad (A13)$$

For given spectral type and luminosity class of the star and for empirically determined values of $\chi_{\mathrm{C\,II}}$, values of ℓ can be obtained from Eq. (A12). These must satisfy $\ell \geq \min\ell$ for the values of $\min f_{\mathrm{beam}}$ implied by Eq. (A6) [root must be real], yielding estimates of f_{beam}. Values of $F(G_0)$ are then given by Eqs. (A4) and (A13). Similarly, the vector r can be constructed from Eqs. (A3) and (A5) and its direction cosine from Eq. (A6).

References

Abergel A., Bernard J.P., Boulanger F., et al., 1996, A&A 315, L 329
Abergel A., Bernard J.P., Boulanger F., et al., 1998, In: Yun J.L., Liseau R. (eds.) Star Formation with the Infrared Space Observatory. ASP Conf.Ser., 132, p. 220
André P., Ward-Thompson D., Barsony M., 1993, ApJ 406, 122
Bakes E.L.O., Tielens A.G.G.M., 1998, ApJ 499, 258
Bell K.L., Berrington K.A., Thomas M.R.J., 1998, MNRAS 293, L 83
Bertoldi F., 1998, A&A, preprint
Bohlin R.C., Savage B.D., Drake J.F., 1978, ApJ 224, 132
Boulanger F., Reach W.T., Abergel A., et al., 1996, A&A 315, L 325
Bragg S.L., Brault J.W., Smith W.H., 1982, ApJ 263, 999
Burton M.G., Hollenbach D.J., Tielens A.G.G.M., 1990, ApJ 365, 620
Casanova S., Montmerle T., Feigelson E.D., André P., 1995, ApJ 439, 752
Ceccarelli C., Haas M.R., Hollenbach D.J., Rudolph A.L., 1997, ApJ 476, 771
Cesarsky C.J., Abergel A., Agnèse P., et al., 1996, A&A 315, L 32
Chini R., 1981, A&A 99, 346
Clegg P.E., Ade P.A.R., Armand C., et al., 1996, A&A 315, L 38
Draine B.T., Bertoldi F., 1996, ApJ 468, 269
Ferland G.J., 1996, *Hazy*, a Brief Introduction to Cloudy 90. University of Kentucky, Physics Department Internal Report
Ferland G.J., Korista K.T., Verner D.A., et al., 1998, PASP 110, 761
Frerking M.A., Keene J., Blake G.A., Phillips T.G., 1989, ApJ 344, 311
Frerking M.A., Langer W.D., Wilson R.W., 1982, ApJ 262, 590
Galavís M.E., Mendoza C., Zeippen C.J., 1997, A&AS 123, 159
Gómez M., Whitney B.A., Wood K., 1998, AJ 115, 2018
Greene T.P., Young E.T., 1989, ApJ 339, 258
Habing H.J., 1968, Bull. Astr. Inst. Netherlands 19, 421
Hanner M.S., Brooke T.Y., Tokunaga A.T., 1995, ApJ 438, 250
Hollenbach D., McKee C.F., 1989, ApJ 342, 306
Hollenbach D., Natta A., 1995, ApJ 455, 133
Hollenbach D.J., Tielens A.G.G.M., 1997, ARA&A 35, 179
Hollenbach D.J., Takahashi T., Tielens A.G.G., 1991, ApJ 377, 192
Jaquet R., Staemmler V., Smith M.D., Flower R.D., 1992, J. Phys. B: At. Mol. Opt. Phys. 25, 285
Kaufman V., Sugar J., 1986, J. Phys. Chem. Ref. Data 15(1), 321
Keenan F.P., Conlon E.S., Rubin R.H., 1994, ApJ 434, 811
Kessler M.F., Steinz J.A., Anderegg M.E., et al., 1996, A&A 315, L 27
Kurucz R.L., 1992, In: Barbuy B., Renzini A. (eds.) The Stellar Populations of Galaxies. IAU Symp. 149, p. 225
Lada E.A., Strom K.M., Myers P.C., 1993, In: Levy E.H., Lunine J.I. (eds.) Protostars and Planets III. Univ. Arizona Press, p. 245
Launay J.M., Roueff E., 1977, A&A 56, 289
Liseau R., Lorenzetti D., Molinari S., et al., 1995, A&A 300, 493
Loren R.B., Wootten A., Sandqvist Aa., Bernes C., 1980, ApJ 240, L 165
Loren R.B., Wootten A., Wilking B.A., 1990, ApJ 365, 269
Maloney P.R., Hollenbach D.J., Tielens A.G.G.M., 1996, ApJ 466, 561
Monteiro T.S., Flower R.D., 1987, MNRAS 228, 101
Motte F., André P., Neri R., 1998, A&A 336, 150
Rentzsch-Holm I., Holweger H., Bertoldi F., 1998, In: Yun J.L., Liseau R. (eds.) Star Formation with the Infrared Space Telescope. ASP Conf. Ser. 132, p. 275
Saraceno P., Nisini B., Benedettini M., et al., 1998, In: Yun J.L., Liseau R. (eds.) Star Formation with the Infrared Space Observatory. ASP Conf.Ser. 132, p. 233
Savage B.D., Mathis J.S.,, 1979, ARA&A 17, 73
Savage B.D., Sembach K.R., 1996, ARA&A 34, 279
Shu F.H., Adams F.C., Lizano S., 1987, ARA&A 25, 23
Spaans, M, 1996, A&A 307, 271
Störzer H., Hollenbach D., 1998, ApJ 495, 853
Störzer H., Stutzki J., Sternberg A., 1996, A&A 310, 592
Swinyard B.M., Clegg P.E., Ade P.A.R., et al., 1996, A&A 315, L 43
Tielens A.G.G.M., Hollenbach D.J., 1985a, ApJ 291, 722
Tielens A.G.G.M., Hollenbach D.J., 1985b, ApJ 291, 747
Vrba F.J., Coyne G.V., Tapia S., 1993, AJ 105, 1010
Whittet D.C.B., van Breda I.G., Glass I.S., 1976, MNRAS 177, 625
Wilking B.A., Lada C.J., 1983, ApJ 274, 698
Wilking B.A., Lada C.J., Young E.T., 1989, ApJ 340, 823
Wilking B.A., Schwartz R.D., Fanetti T.M., Friel E.D., 1997, PASP 109, 549
Wright E.L., Mather J.C., Bennett C.L., et al., 1991, ApJ 381, 200
Yui Y.Y., Nakagawa T., Doi Y., et al., 1993, ApJ 419, L 37